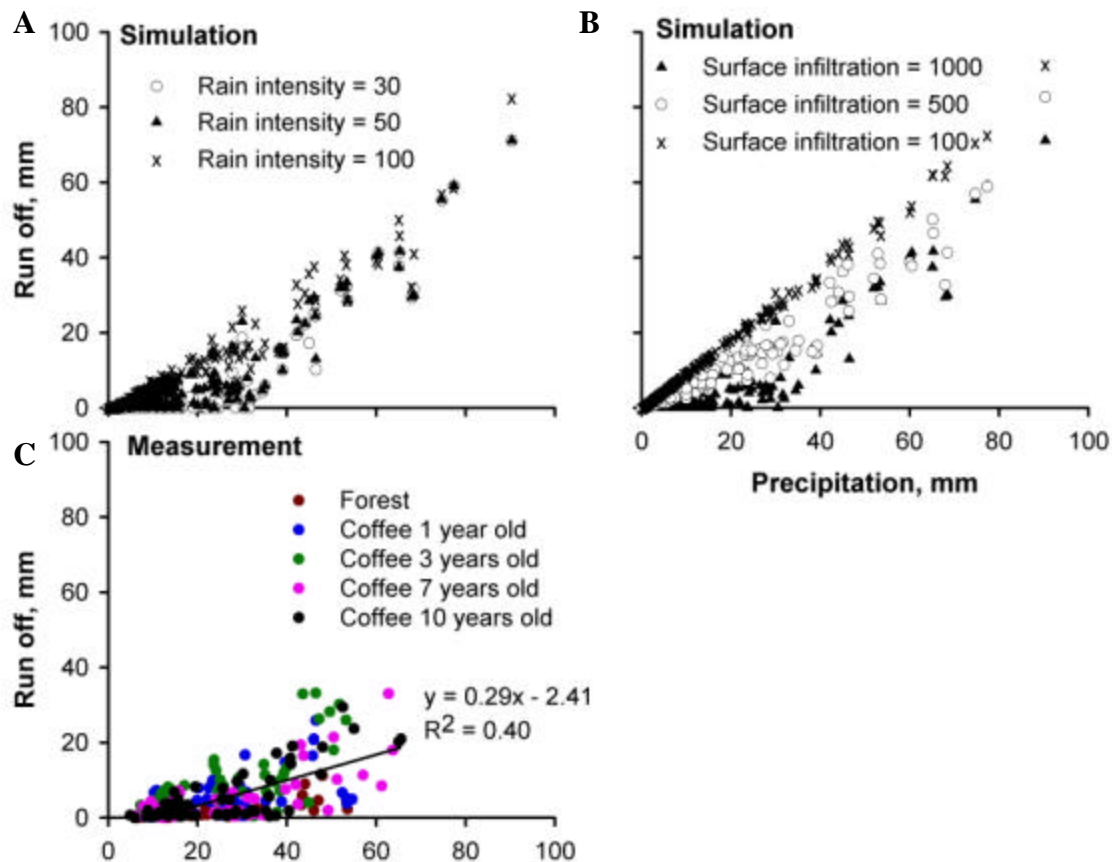


We conclude that the difference in model predictions on a daily scale between versions that are based on detailed parameterization and versions based on coarser estimates do not lead to problems when longer time frames are considered, except for differences in overland flow. For other processes the temporary storage of water in soil leads to strong compensatory effects: an overestimate of a uptake or drainage on a given day will lead to a ‘self-correcting’ underestimate on the following days. Correct prediction of the infiltration versus surface runoff fate of water that reached the soil surface is, however, dependent on the assumptions about soil physical properties, and can influence the results at both daily and longer time steps.

### 3.3.3 Run off in WaNuLCAS

A validation test was made for WaNuLCAS prediction of surface runoff in a ‘chronosequence’ of plots that are supposed to represent changes with time after forest conversion to coffee gardens with ages of 0 – 10 years in Sumberjaya (Way Besai), West Lampung, Indonesia.



**Figure 3.24. A, B.** Sensitivity analysis of WaNuLCAS simulations of run off during a 1 year cycle in 1-year old coffee gardens on 30% slope in Sumber Jaya (Lampung, Indonesia), for variations in mean rainfall intensity (with an assumed coefficient of variation of 0.3; assumed potential rate of surface infiltration 1000 mm day<sup>-1</sup>) and a range of potential surface infiltration rates at a mean rainfall intensity of 50 mm hour<sup>-1</sup>. **C.** Runoff data for small plots in forest and 1-10 year old coffee gardens (unpublished data Brawijaya University)

An earlier version of the model used a mean value of ‘rainfall intensity’ to compare the supply of water at the soil surface with the potential rate of infiltration. Most of the runoff predictions originated from ‘saturation overland flow’, where the rainfall exceeded the antecedent soil water deficit. In a graph of rainfall versus predicted runoff, the model predicted an ‘infiltration intercept’ (an amount that could be absorbed) and a ‘marginal rate of runoff of close to 1 above this intercept. This pattern, a logical consequence of the assumptions, is on contrast with empirical data that tend to show a ‘marginal rate of runoff’ of say 10 – 30% with a smaller intercept (Fig. 3.24 C; the regression analysis suggests a runoff coefficient of 0.29 and an x-axis intercept of 8 mm day<sup>-1</sup>). A ‘broken stick’ interpretation with a larger X-axis intercept and a steeper slope is, however, consistent with the data as well.

Model adjustments that lead to the current WaNuLCAS version have included a statistical distribution function for rainfall intensity. Sensitivity analysis of the model for changes in mean rainfall intensity (Fig.3.24 A) and surface infiltration rate (Fig. 3.24 B) suggest that a rainfall intensity of 30 mm day<sup>-1</sup> (with a coefficient of variation of 0.3) and a potential surface infiltration rate of about 500 mm day<sup>-1</sup> can reproduce the clouds of points that we obtained in the field (the simulations represent a full year, the field data presented here only 3 months).

The main impression these field data may leave behind is that at the scale of the measurement plot there is a large variation between replicates and between rain events of similar total rainfall. At the scale of streams and rivers much of this variation may be reduced and descriptors of the means, such as the regression equation, are acceptable for general trends, but may underestimate ‘local hazard’ at scales below, say, 1 km<sup>2</sup>.

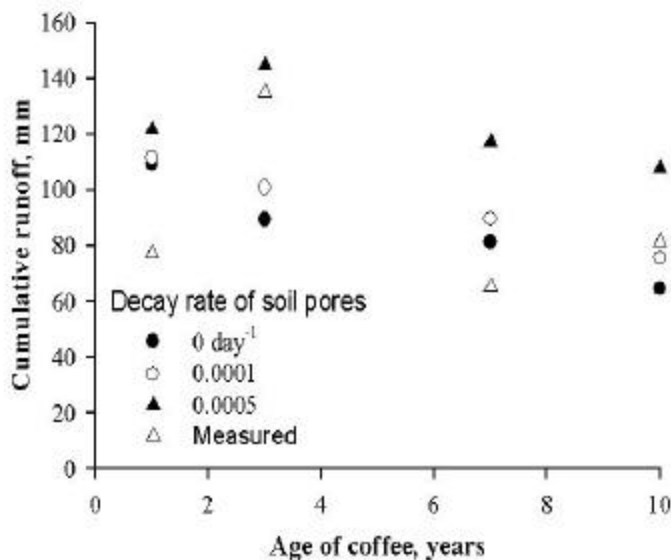


**Figure 3.25.** WaNuLCAS simulations and measured data of surface runoff during a 3-month period, for 3 values of the ‘soil structure decay rate’ (at a decay rate of 0 day<sup>-1</sup> there is supposedly no build up of new structure either)

The ‘chronosequence’ data suggest that important changes occur in runoff after forest conversion, with the highest surface runoff in 3-year-old gardens. The WaNuLCAS model allows to dissect the aboveground and belowground components of these changes:

the growth of coffee plants will lead to a partial recovery of canopy interception and vegetation water use (although not to the level of the original forest), and this will lead to a reduction of surface runoff with time, in a monotonic fashion (filled circles in Fig. 3.22). When we add the concept of a dynamic soil structure, we can obtain the ‘humped’ patterns where surface runoff peaks in 3-year old coffee gardens, as the forest-soil macroporosity has declined and the rebuilding of structure based on surface mulch (litter fall) and biological activity is still in an early phase.

The relatively simple description of soil structure decay and build-up appears to be, at least qualitatively, sufficient to represent the types of changes that the field data suggest. Given the large spread in the data at the individual event level, we cannot expect, at this stage, to have sensitive tests of more elaborate models.

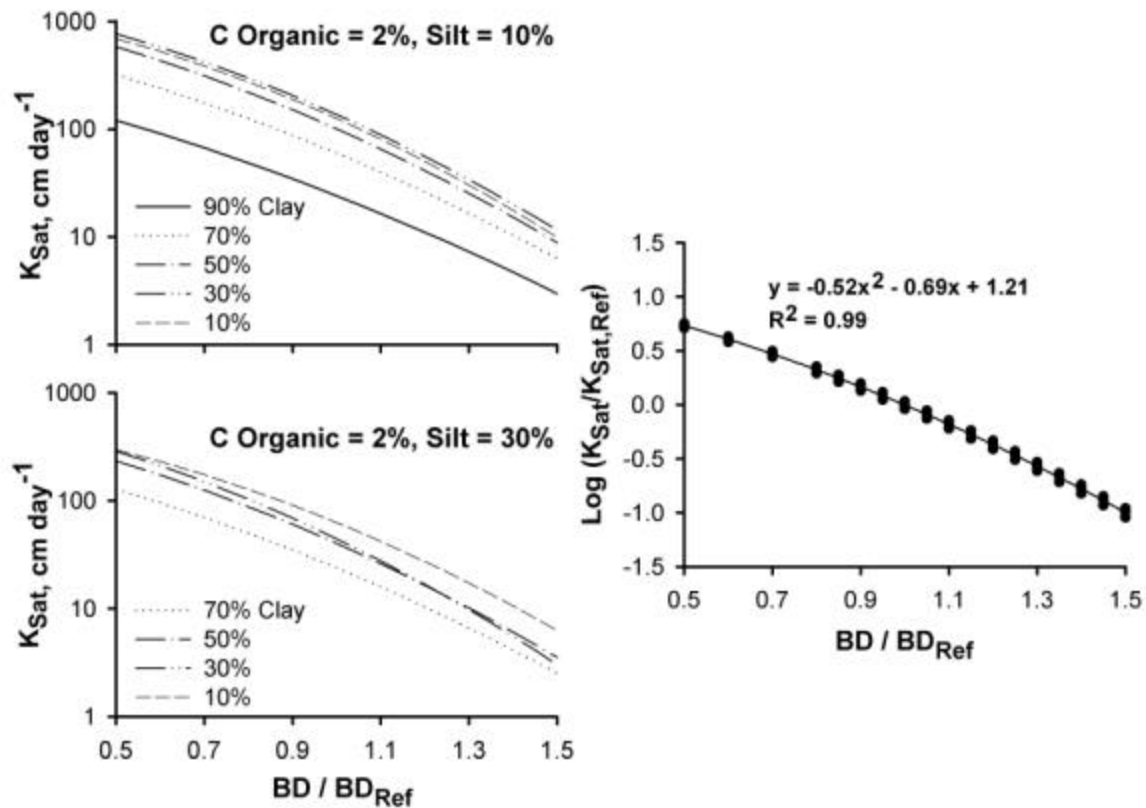


**Figure. 3.26. A, B** Relationship between bulk density of the soil (relative to a reference values derived from agricultural soils of the same texture and soil organic matter content) and the saturated hydraulic conductivity of the soil that is important in the infiltration process, based on the pedotransfer function used in the WaNuLCAS model; dynamic changes in soil structure can be related to equivalent changes in soil conductivity based on the relationship in panel **C**

The pedotransfer model that is used in WaNuLCAS, based on a large but dominantly temperate zone database, suggests a relationship between bulk density of the soil, relative to what one would expect given soil texture and soil organic matter content, and the saturated hydraulic conductivity

In conclusion of this section, we can state that dynamical changes in soil structure after conversion from forest to coffee gardens can be simulated in a way that is consistent with existing field data for Sumber Jaya, building onto global data sets and ‘pedotransfer’ functions. The results can be tested at the level of ‘statistical distributions’ rather than individual events, as key variables such as rainfall intensity during storms and small-range variation in soil structure is only known at the distribution level

### 3.3.4 WaNuLCAS predictions for intensification of crop-fallow systems in northern Thailand

The WaNuLCAS simulation of a series of crop-fallow systems is summarized in Fig. 3.23 and Table 3.4

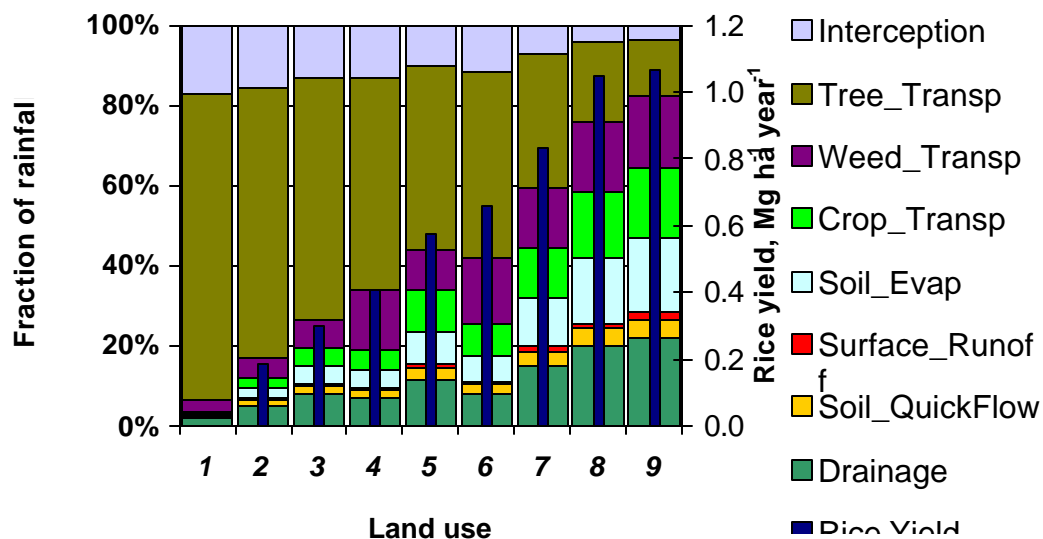


**Figure 3.27** Predictions with the WaNuLCAS model of a series of land use scenarios that represent intensification of crop-fallow systems based on upland rice in northern Thailand (for details of the scenarios see Table 3.4)

Between the 8 scenarios the predicted total yield of rice would increase from 3.6 to 12.8 Mg ha<sup>-1</sup> during 12 years of the various systems. The yield per crop would decline from 1.8 for scenario 5 to 1.4 for scenario 1 – which is substantially above the yield levels recorded and suggest that some limiting factors exist that are not yet represented in the model.

During each cropping cycle crop yields gradually declined, but relatively little. The average decline factor for subsequent crop yields was 10.7% (or 9.7% if a logarithmic average is preferred). Between the individual simulations we found that this decline varied between 5 and 19%, and the use of a single parameter value (as in the FALLOW model) obviously misses out on some of the variation in real world. The relatively slow decline in predicted crop yields is related to the fact that phosphorus (P) rather than nitrogen (N) is predicted to be the dominant nutrient constraint to the growth of upland rice on these soils. The increase in yields after a fallow period is also modest, with predicted yield levels for a first crop declining only from 1.9 Mg ha<sup>-1</sup> for the

most extensive scenario tested (scenario 5) to 1.5 Mg ha<sup>-1</sup> for the most intensive one (scenario 1).

**Table 3.4.** WaNuLCAS simulation results for a period of 12 years that is made up of different lengths of fallow (F) and cropping (C) periods. Trees start growth at day 280 in the years specified. Slash-and-burn clearing cycles start at day 340 in the years indicated. Crop growth (upland rice with 70 days of vegetative and 90 days of generative growth) starts at day 120 in the years indicated. Mean rainfall over 12 years: 1215 mm year<sup>-1</sup>

Scenario	0	1	2	3	4	5	6	7	8
Code	F	1*(1 1F+1 C)	1*(1 0F+2 C)	2*(5 F+1C )	2*(4 F+2C )	3*(3 F+1C )	3*(2 F+2C )	4*(1 F+2C )	3*(1 F+3C )
Ruthenberg factor	0	0.08	0.17	0.17	0.33	0.25	0.5	0.67	0.75
T_start year	0	0	0, 11	0, 6	0, 5, 11	0, 4, 8	0, 3, 7, 11	0, 2, 5, 8, 11	0, 3, 7, 11
S&B year		10	9	4, 0	3,9	2, 6, 10	1, 5, 9	0, 3, 6, 9	0, 4, 8
Crop year		11	10,11	5, 11	4,5,1 0,11	3, 7, 11	2,3,6, 7,10, 11	1,2,4, 5,7,8, 10,11	1,2,3, 5,6,7, 9,10, 11
<b>Water balance</b>									
<b>(%)</b>									
Interception	17.1	15.6	13	13.3	10	11.7	7	4.4	3.6
Surface_Runoff	0.6	0.4	0.7	0.8	0.9	0.6	1.2	1.4	1.9
Soil_QuickFlow	0.2	1.3	1.9	2	2.8	2.2	3.5	4.5	4.9
Drainage	2.2	5.1	7.8	6.8	11.6	8.2	15	19.7	21.7
Soil_Evap	0.5	2.5	4.6	4.6	8.1	6.3	11.9	16.3	18.3
Crop_Transp	0.0	2.4	4.4	4.9	10.4	8	12.6	16.3	17.4
Weed_Transp	2.9	5.1	6.9	14.8	10.1	16.8	15.2	17.6	18
Tree_Transp	76.6	67.6	60.7	52.9	46.1	46.2	33.4	19.7	14.1
<b>Agronomic yields</b>									
Rice yield, Mg ha <sup>-1</sup> year-1	0	0.18	0.30	0.41	0.58	0.66	0.83	1.05	1.07
Days of work/ha	0	249	251	458	654	668	867	1061	859
First crop yield, Mg ha <sup>-1</sup>	0	2.21	1.89	2.45	1.73	2.74	1.76	1.68	1.51
kg rice/day of work	0.0	8.7	14.3	10.7	10.6	11.8	11.5	11.9	14.9

It is generally thought that crop yield decline is associated with decreasing soil fertility and increasing weed infestation. However, it was shown that soil organic matter content in the early and late fallow fields in a chronosequence study of soil fertility in the forest-fallow shifting cultivation system were comparable (Wangpakapattanawong, 2001). Therefore, it is unlikely in this system that soil fertility decline linked to N supply is a major contributing factor of yield reduction in subsequent cropping.

Across the five scenarios the total water yield was predicted to increase substantially with increasing cropping ratio, but there is little change in partitioning over ‘peak flow’ and ‘base flow’; 75-77% of total water yield is expected to come as ‘base flow’ through a deep soil pathway, and 23-28% of the ‘peak flow’ is expected via a surface runoff pathway, with the remainder (72-77%) via a subsurface lateral flow or ‘soil-quick flow’ pathway.

### 3.4 SpatRain experiments

Daily rains were generated using SpatRain across the meso-scale catchment area of Sumberjaya, Lampung, Sumatra (about 500 km<sup>2</sup>), which is formed by 15 sub catchments based on contributory streams identified by a digital elevation model, using a grid resolution of 1 km<sup>2</sup> (Figure 3.28). Existing rainfall data for this area were analyzed for spatial patterns by Manik and Sidle (2003). Eighteen points were chosen randomly across the catchment to check simulated cell-level rainfall sequences. Actual daily records were obtained from 21-year time series of one station, which is located 3.5 km from the catchment center (*i.e.* Pajarbulan; other rainfall stations have shorter time series but are probably not significantly different in means or variance measures (Figure 3.13); Manik and Sidle (2003)).

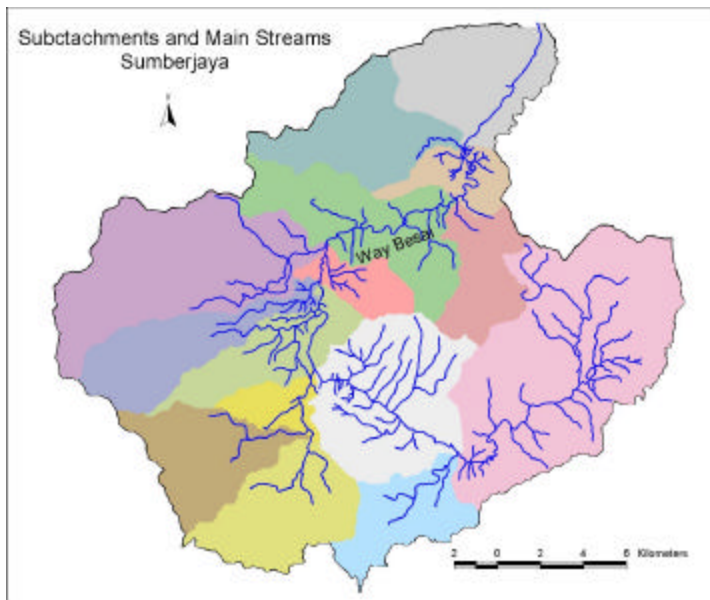


**Figure 3.28.** Sumberjaya catchment in Lampung, Sumatra as formed by 15 subcatchments. This catchment was used to test the model.

Parameter values used to generate various types of rainfall in this experiment are listed in Table 3.5. Patchy rains were characterized by individual storm with extremely small core area (radius of 1 km and core width of 1 km) and with extremely narrow distribution on its intensity ( $f^{\rightarrow}/f^{\leftarrow}$  combination of 1/100), whereas homogeneous rains were characterized by individual storm with very large core area (radius of 20 km and core width of 10 km) and with very spreading distribution on its intensity ( $f^{\rightarrow}/f^{\leftarrow}$  combination of 1/100). In between, intermediate rains were expected to be formed by storm radius of 11 km, core width of 11 km and  $f^{\rightarrow}/f^{\leftarrow}$  combination of 1/50.

**Table 3.5.** Parameters used for SpatRain experiments. All values formed compatible storms with the observed station records.

Parameters	Patchy	Intermediate	Homogeneous
Radius of trajectory of individual storm (km)	1	11	20
Core width of individual storm (km)	1	11	10
Spreading factor of intensity distribution from the core, $f^{\rightarrow}$	1	1	100
Agglomerating factor of intensity distribution from the core, $f^{\leftarrow}$	100	50	1

Figure 3.25 shows the simulated daily rain maps of patchy, intermediate and homogeneous storms generated by SpatRain. Table 3.6. shows that low wet fraction of patchy rains in space was compensated by high events probability in time. It also tells that equation  $P|\ddot{a}| = P|\div|^N$  and  $N = \frac{\ln(1-d)}{\ln(1-c_1)}$  (see part 2.2.5) can generate a sensible range of N that produce a sensible range of wet cells fraction  $c_N$  at such patchy condition, as indicated by cross scale probability of storm events  $P(E_N) \leq 1$ . This cross scale probability of storm events acts similarly to the  $\lambda$  value in Poisson distribution that represents permutation of rainfall events in time scale (Rodriguez –Iturbe et al., 1987).

**Table 3.6.** Cross scale properties of homogenous (h), intermediate (i) and patchy (p) rainfalls

Month	Storm events number (N)			Wet cell fraction of N storm events ( $c_N$ )			Probability of storm event ( $P(E_N)$ )		
	<i>h</i>	<i>i</i>	<i>p</i>	<i>h</i>	<i>i</i>	<i>p</i>	<i>h</i>	<i>i</i>	<i>p</i>
<b>Jan</b>	1	2	46	1	0.66	0.48	0.34	0.52	0.71
<b>Feb</b>	1	2	39	1	0.40	0.39	0.30	0.74	0.77
<b>Mar</b>	1	2	37	1	0.46	0.40	0.28	0.62	0.71
<b>Apr</b>	1	2	33	1	0.64	0.30	0.26	0.40	0.85
<b>May</b>	1	2	30	1	0.45	0.35	0.24	0.54	0.69
<b>Jun</b>	1	1	19	1	0.43	0.30	0.16	0.37	0.53
<b>Jul</b>	1	1	15	1	0.31	0.26	0.13	0.43	0.51
<b>Aug</b>	1	1	18	1	0.44	0.33	0.15	0.34	0.46
<b>Sep</b>	1	1	17	1	0.27	0.14	0.14	0.53	0.98
<b>Oct</b>	1	1	21	1	0.21	0.23	0.17	0.81	0.74
<b>Nov</b>	1	2	37	1	0.59	0.37	0.29	0.48	0.78
<b>Dec</b>	1	1	26	1	0.40	0.29	0.21	0.52	0.72

The simulation results shows that temporal distribution of patchy and intermediate rainfalls from 18 sampled points are diverse but still consistent with the actual station records distributions (Figure 3.26), with gradual skewness at subcatchment distributions and subsequently at catchment-levels distributions while homogeneous rainfalls have the same distributions from cell- to catchment-levels (Fig. 3.27). As a consequence, patchy rainfalls have relatively low inter-annual variability (Figure 3.28), with coefficient of variance of 10.04% at cell-level, compared to the intermediate (11.51%) and the

homogeneous (16.79% that is closed to the actual of 17.68%). This may suggest that probability of cells hit by storm cores is not uniform, as it is now assumed by SpatRain, but is likely driven by multi-step Markov process (Jones and Thornton, 1997), which tells that probability of today rain events are driven by rain events occurred before. Thus, a ‘memory’ parameter should be introduced into the model to keep track the dynamics of cell probability hit by the storm if one expects to compare the effect of rainfall patchiness at the same degree of inter-annual variability.

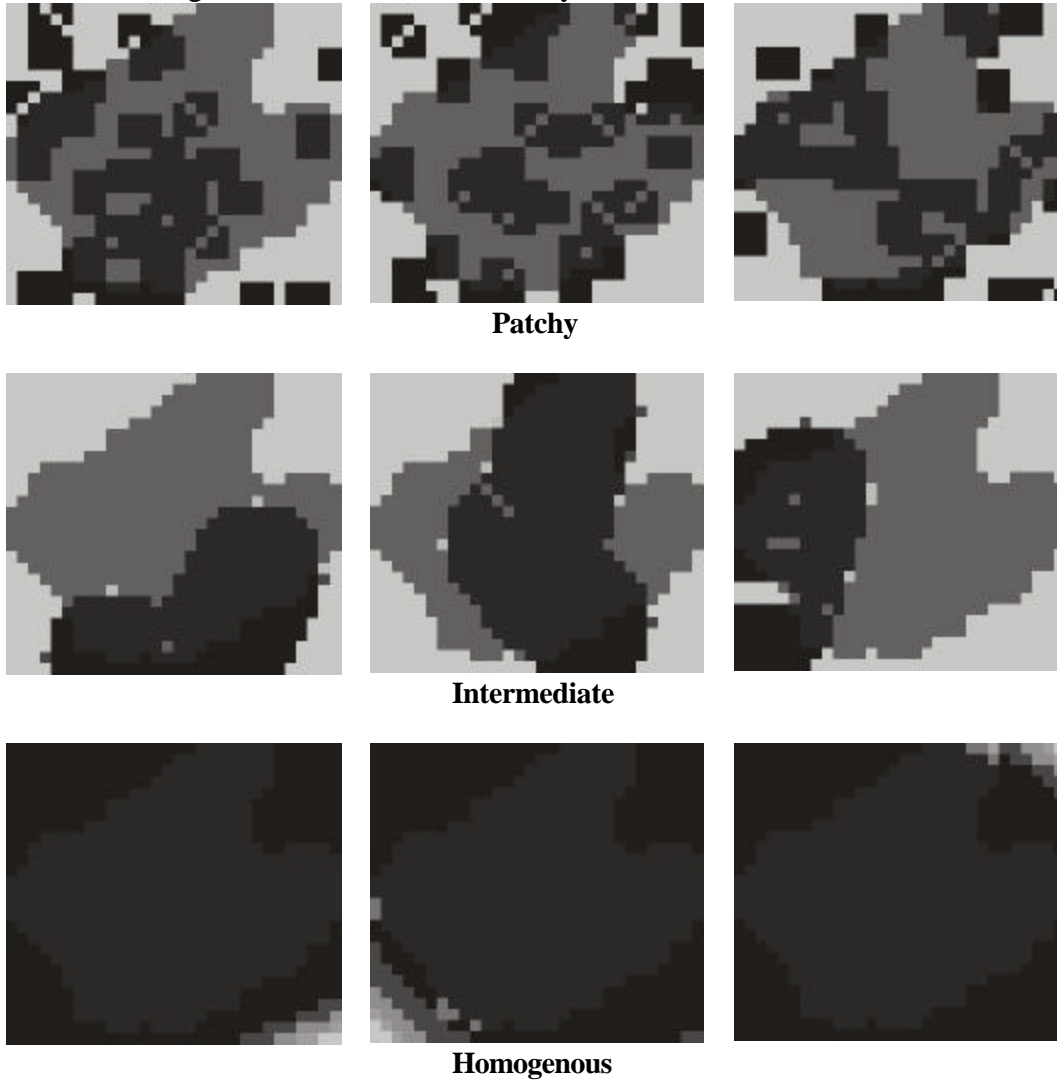
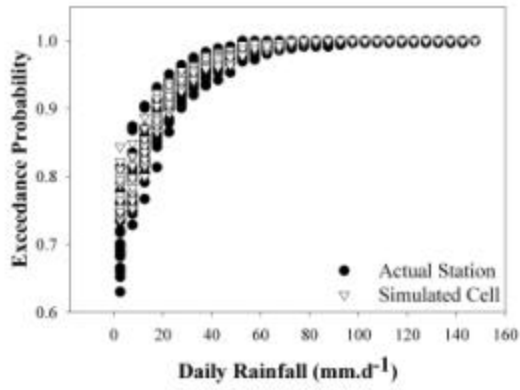


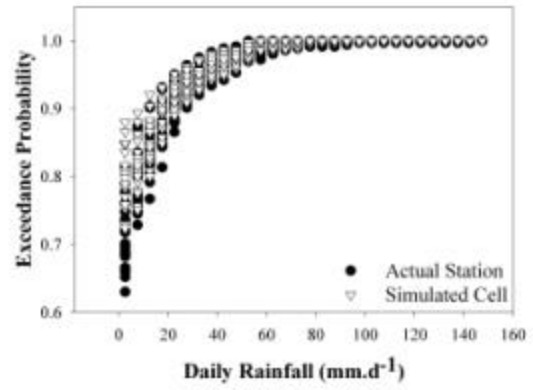
**Figure 3.29.** Simulated daily rainfall maps. Dark area indicates storm cores that hit or miss the catchment area.

Simpler way to overcome inter-annual variability problem is by doing data segmentation to derive the station exceedance probability ( $f$ ) into dry band ( $x_t < |\mu - w \cdot \delta|$ ), normal band ( $|\mu - w \cdot \delta| \geq x_t \leq |\mu + w \cdot \delta|$ ) and wet band ( $x_t > |\mu + w \cdot \delta|$ ), where  $x_t$  is annual rainfall of data series in the year- $t$  (mm),  $\mu$  and  $\delta$  are year average and standard deviation of annual rainfall (mm), and  $w$  is range width multiplier of the normal band. Such data segmentation can be incorporated as option within the program and simulation can be based on ENSO scenarios. Figure 3.29 shows that inter-annual variability in simulated

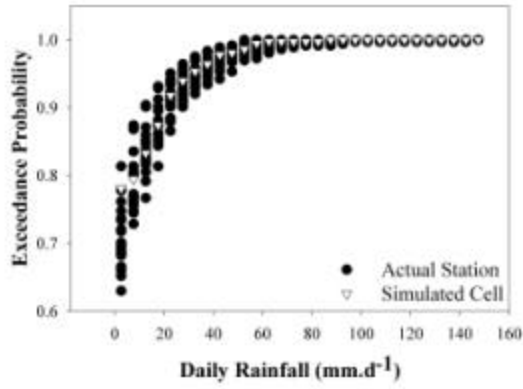
rainfalls with homogeneous pattern can be obtained by data segmentation to derive f into 3 different bands.



**Patchy**

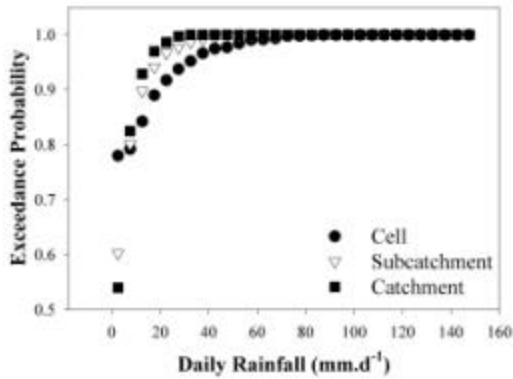


**Intermediate**

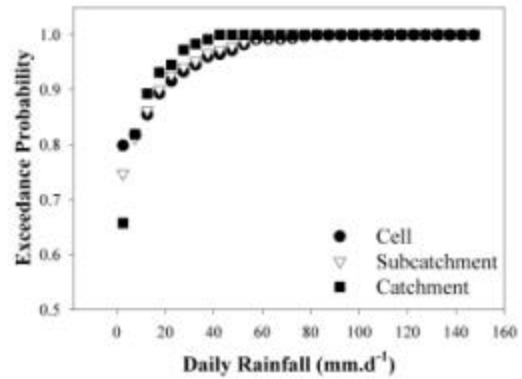


**Homogeneous**

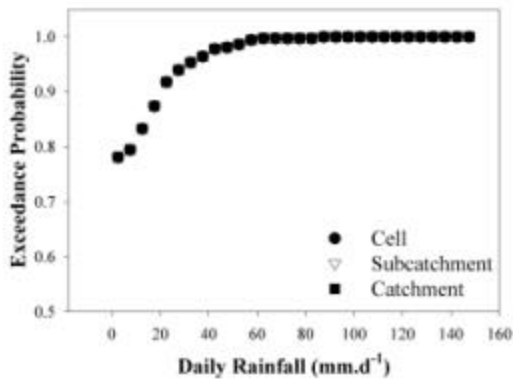
**Figure 3.30.** Distribution consistency of simulated rainfalls to the actual distribution



**Patchy**

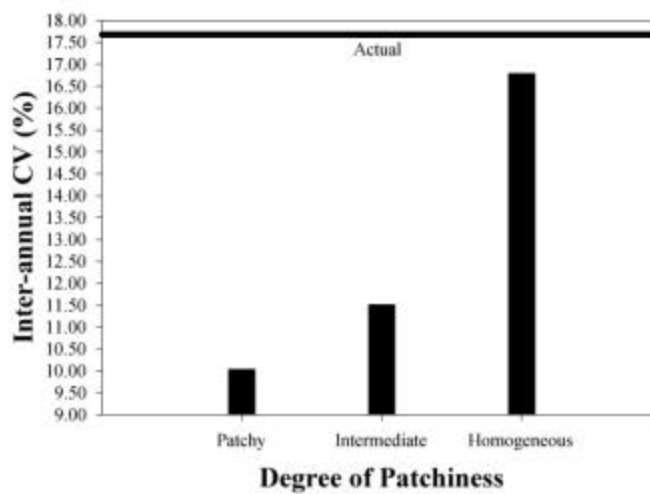


**Intermediate**

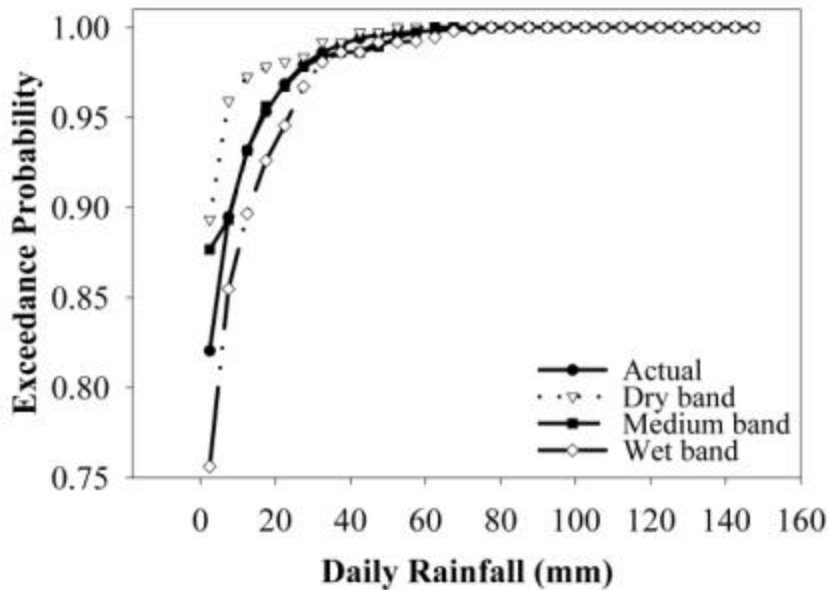


**Homogeneous**

**Figure 3.31.** Distribution skewness from cell- to subcatchment and catchment-levels of simulated patchy and intermediate rainfalls, whereas homogeneous rainfalls have the same distribution from cell- to catchment-levels.



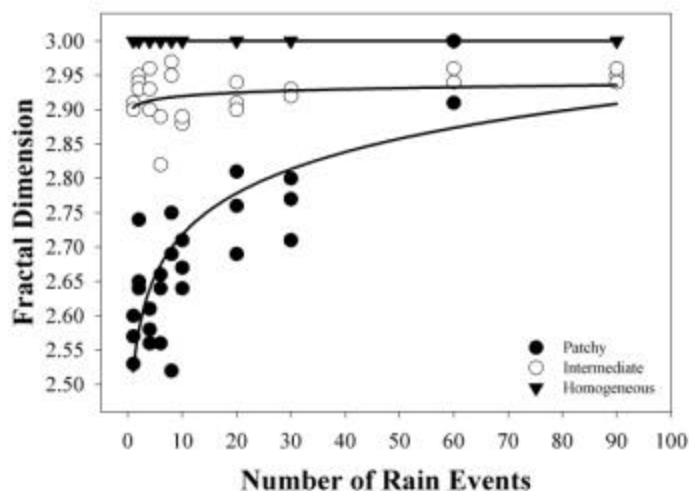
**Figure 3.32.** Inter-annual variability of simulated rainfalls at various degrees of patchiness, compared to the actual.



**Figure 3.33.** Simulation results after data segmentation into dry, normal and wet bands.

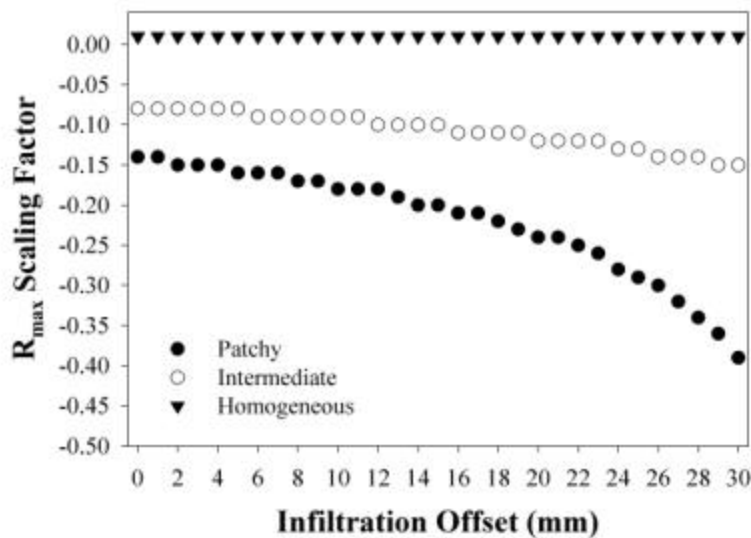
Fractal dimension was used as patchiness indicator, derived from semivariogram's slope. Fitting-curve of  $y = a(1 - e^{-bx})$  was used to estimate the slope. If we took 1 rain event as the reference map for semivariance analyses, we got fractal dimension of about 2.57, 2.91 for and 3.00 in average for patchy, intermediate and homogeneous rainfalls respectively. Thus, in term of its patchiness indicator, the assumed intermediate rainfalls in this experiment are in fact 79% homogeneous.

Figure 3.30 shows that temporal averaging increased the patchiness of patchy rainfalls, so that it approached the patchiness of intermediate and homogeneous rainfalls starting from temporal averaging of 30 rain events. This result gives more explanation on low spatial autocorrelation of monthly rainfall between stations as studied by Manik and Sidle (2003). We will show the effect of such averaging in some parts about GenRiver.

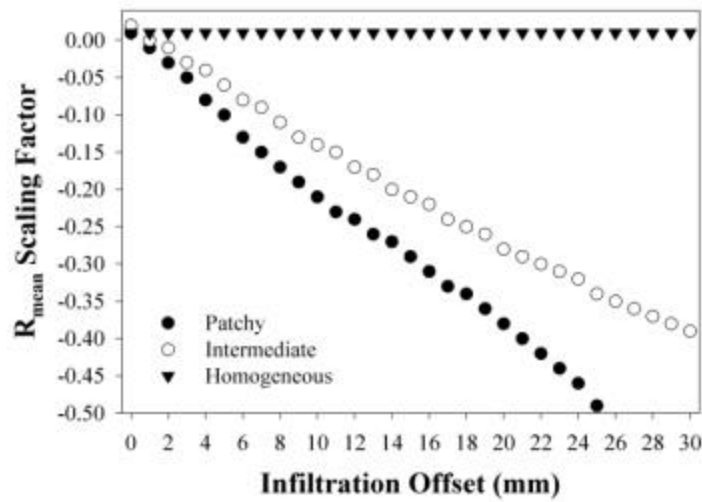


**Figure 3.34.** Effects of temporal averaging on rainfall patchiness.

Spatial scaling properties of maximum daily rainfall ( $R_{\max}$ ) and average daily rainfall ( $R_{\text{mean}}$ ) over 1 year period of patchy, intermediate, and homogeneous rainfalls were explored by conducting resampling (window averaging) to simulated data at various sizes of windows, ranging from 1 km<sup>2</sup> to the maximum trajectory area of 810 km<sup>2</sup>. Infiltration offsets from 0 mm to 30 mm were introduced into resampled maps with regards to the intercept of precipitation-runoff relation as explored by WaNuLCAS Model (Figure 3.20). Figure 3.34 shows that scaling factor of  $R_{\max}$  can approach the scaling factor of maximum river flow per area ( $Q_{\max}/A$ ) of  $-0.25$ , as reviewed by Rodriguez–Iturbe and Rinaldo (1997), only by patchy rainfalls at infiltration offset of 22 mm. While scaling factor of  $R_{\text{mean}}$  can approach the scaling factor of mean annual discharge per area ( $Q_{\text{mean}}/A$ ) of 0 at patchy rainfall condition without infiltration offset. Where total water yield is likely to be independent of an infiltration offset, we conclude that a consistent interpretation of the empirical scaling relationships for maximum daily flow and mean annual water yield is feasible. In addition to the spatial properties of rainfall, which are normally used in ‘explaining’ the scaling rules, however, we suggest that the scaling rule depends on the intercept of the rainfall – surface runoff relationship. This dependency makes it likely that the scaling rule for maximum daily flows can be influenced by changes in land use and land cover.



A



B

**Figure 3.35.** Scaling behavior of maximum daily rainfall (A) and mean annual rainfall (B) at various infiltration offsets.

### 3.5 GenRiver exploration of land use change impacts on river flow

#### 3.5.1 Annual water balance for Way Besai and Mae Chaem

The overall water balance for Way Besai (Sumberjaya) and Mae Chaem as simulated with GenRiver (Fig. 3.36) indicates similarities as well as differences. Cumulative evapotranspiration is only slightly less in Mae Chaem than in the Way Besai, but it represents roughly 50 and 85% of the cumulative rainfall, respectively. Cumulative discharge (which equals the sum of Cumulative base flow (CumBaseFlow), surface quick flow (CumSurfQFlow) and soil quick flow (CumSoilQFlow)) is approximately equal to cumulative rainfall (CumRain) minus cumulative evapotranspiration (CumEvapTrans). Evapotranspiration (plus river flow) and rainfall can be partially out of phase, as reflected in the

‘delta catchment storage’ term that ends the year at approximately zero in both simulations.

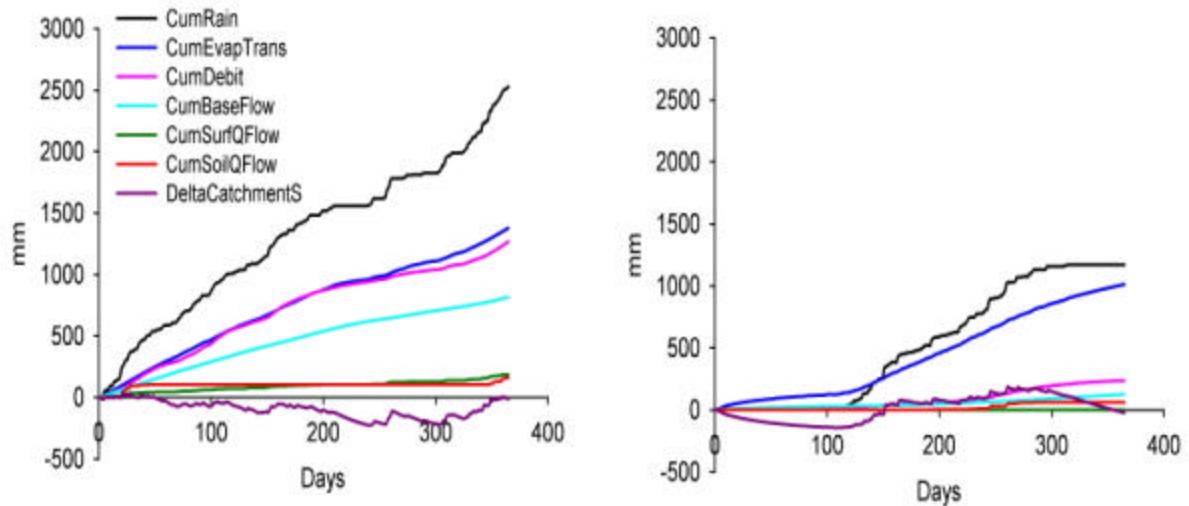


**Figure 3.36** Cumulative water balance as output of GenRiver using Way Besai (Sumberjaya) (A) and Mae Chaem (B) data, for the current land use mosaic in both catchments

In general the terms other than rainfall show a smoother profile of increments, reflecting the buffering conveyed by soil and river system. In the current simulations discharge in the Way Besai consists largely of base flow, with soil quick flow and surface quick flow (derived mainly from December and January rainfall events) making approximately equal contributions to the rest. The Mae Chaem simulations also suggest base flow to be the largest share of river discharge, but surface quick flow is supposed to be a very small term and soil quick flow the dominant mechanism. The Mae Chaem simulation is especially sensitive to changes in the assumptions regarding water use by different land use types, the Way Besai simulation mainly to changes in soil parameters affecting the partitioning between the various flow pathways.

### **3.5.2 GenRiver simulation using two different type of rainfall**

Using two different types of rainfall generated by SpatRain, we simulated river flow for Way Besai, Sumberjaya. Result are here shown for the beginning (year 3) and end (year 20) of the simulation (year 3 is shown since we found that result for the first year depended on initialization of a number of parameters). Year 3 and year 20 of the time series reflecting land cover fractions of 58 and 14% for forest and 22 and 11% for cropland and pioneer stages of fallow vegetation and 12 and 70% for coffee gardens, respectively.

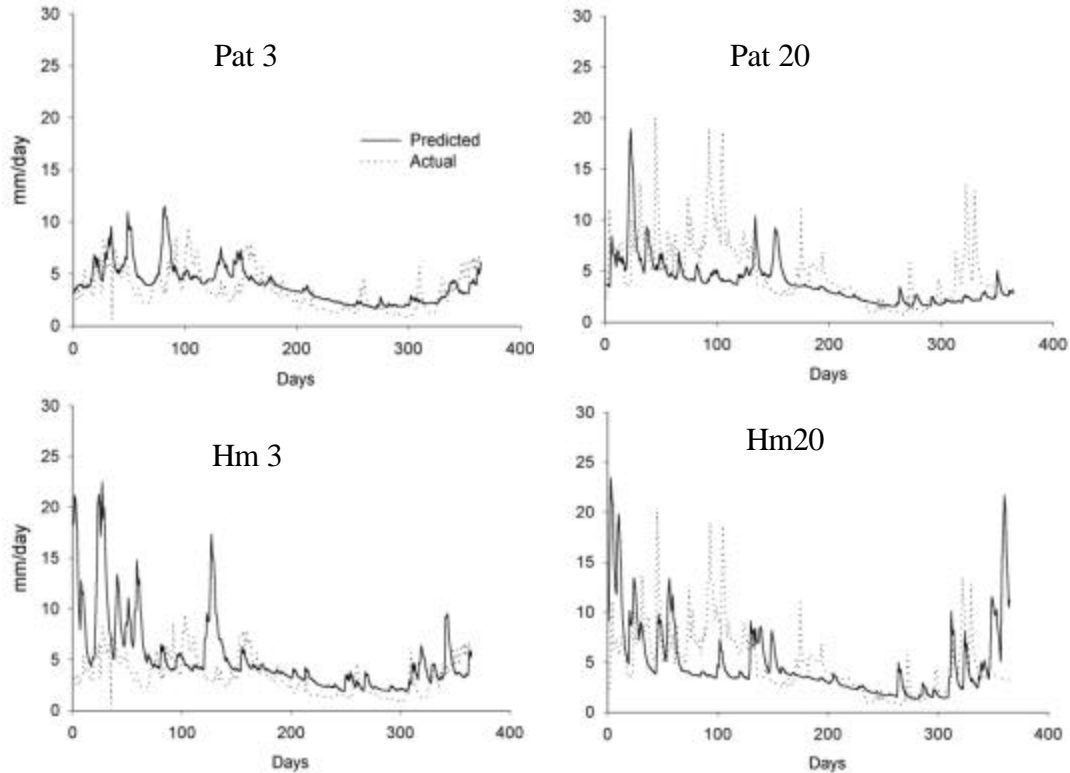


**Figure 3.37.** Measured (dots) and predicted (lines) river flow of Way Besai, Sumberjaya (mm day<sup>-1</sup>) in year 3 and year 20 for patchy and homogenous rainfall pattern.

In the Way Besai simulation patchy rainfall produces a better match of simulated and measured patterns of river flow compared to more homogenous rainfall patterns. We don't expect the simulations to match the dates of the peaks in measured flow (as we started from a resampling of the statistical distribution rather than specific time-series), but we expect the shapes and intensities of highs and the recession during low flow periods to match. A simple test is formed by a comparison of measured and predicted frequency distribution of daily flows during a year (Fig. 3.38).

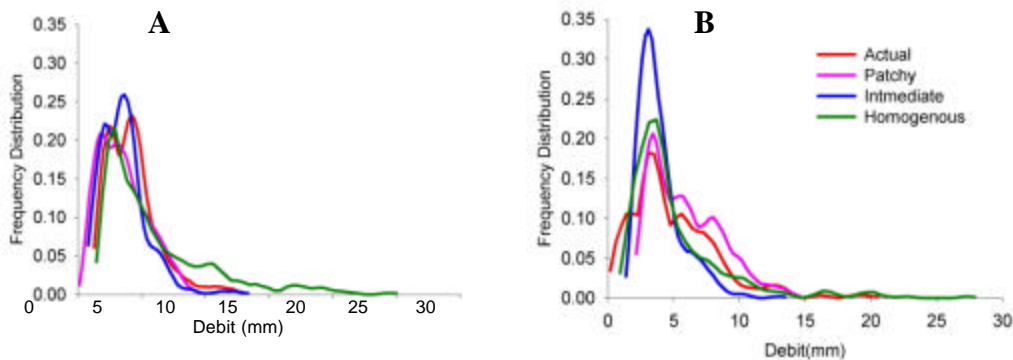


**Figure 3.38.** Frequency distribution of the river discharge, actual and simulated by GenRiver driven by patchy and homogenous rainfall pattern for year 3 (A) and year 20(B) in Way Besai

For the two years selected for this analysis, the frequency distribution of measured river flow matches most closely with the ‘patchy’ rainfall simulation(Fig.3.38).

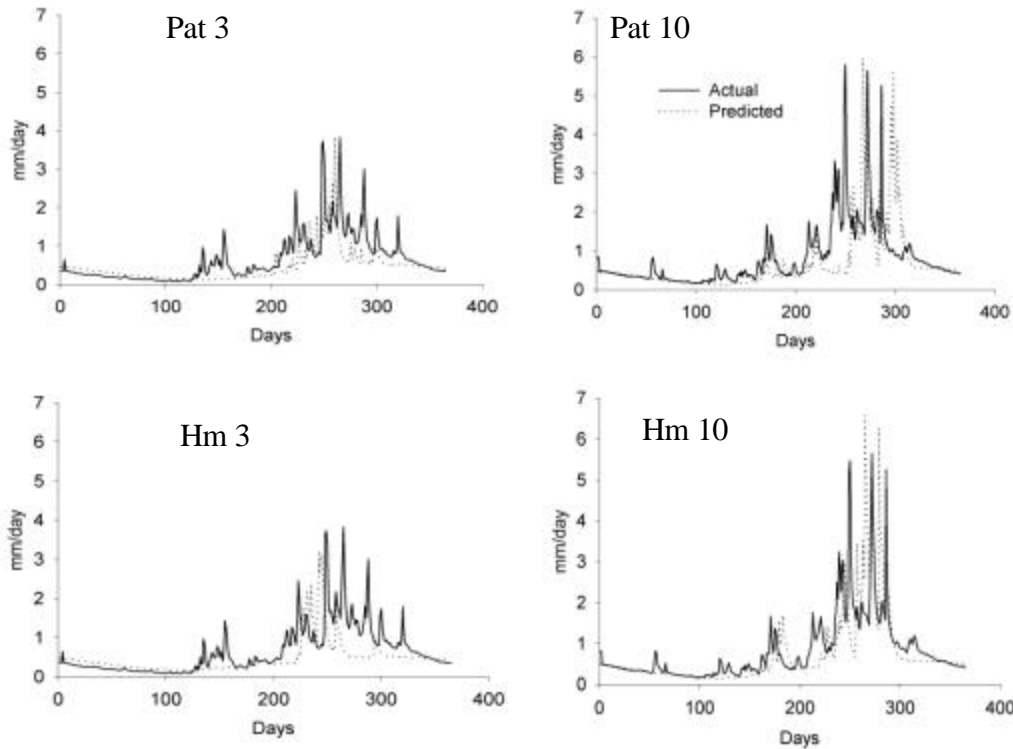


**Figure 3.39.** Actual (dots) and predicted (line) river flow of Mae Chaem in year 3 and year 10 for patchy and homogenous rainfall pattern

For the Mae Chaem simulation we also compared the two rainfall patterns, but the ‘patchy’ rain required a high number of small storms per day to match the target frequency of rain at station level; after aggregation at subcatchment scale the resulting pattern may in fact have been rather homogenous. The results shown here are again for the beginning and end of the simulated series, in year 3 and year 10, both with about 44% of the land under deciduous forest cover, 13% of evergreen forest, 8% of fallow system and 5% of orchard (and the remaining in smaller categories). The simulations found in fact very little difference between the patchy and the homogenous rainfall simulations. For year 3 the match with measured data is fine, for year 10 the pattern looks similar in Fig. 3.39, but the test of frequency distribution suggest a difference (Fig.3.40).

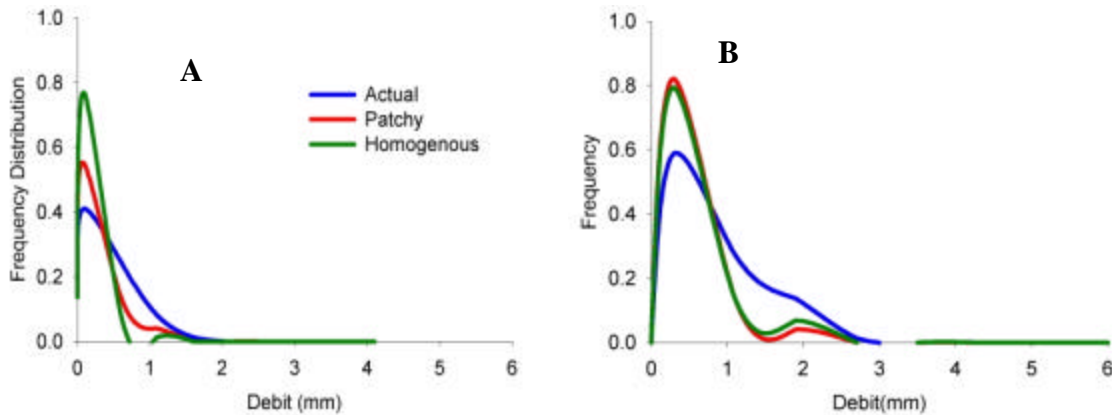


**Figure 3.40.** Frequency distribution of river debit, actual and simulated by GenRiver using patchy and homogenous rainfall pattern for year 3 (A) and year 10 (B)

The buffering indicator (above average river flow per unit above average rainfall) provides a further test of the model versus measurements. To match the actual time series simulated rainfall data were sorted on the basis of total catchment level rainfall and matched with the available station level data. Calculated buffer indicators (Fig. 3.41) for the Way Besai under the ‘current LU mix’ scenario are higher than the measured ones. For Mae Chaem the results suggest a good match with the measured time series.

If we accept the current parameterization of the model for both catchments (in the absence of fine tuning of all available model parameters), we can explore the simulations for an ‘all forest’ and an ‘degraded lands/grassland’ scenario with the current land use mix. As shown in Fig 3.41 these three scenarios consistently ranked the current LU mix between an ‘all forest’ and an ‘all grass’ scenario for both catchments. When we compare the mean buffering indicator across the simulation period (Fig. 3.42), we see that the current LU mix is closer to the ‘all forest’ than it is to the ‘all grass/degraded lands’ scenario, in both catchments. For the Way Besai data we see that patchy rain leads to a higher buffer indicator than simulation with a more spatially homogenous rainfall, as in the patchy rain case the river can provide more buffering by integration across subcatchments. For the Mae Chaem series we, again, found less difference between the two rainfall patterns. Analysis of the frequency distributions of annual buffer indicator values (Fig. 3.43) confirms the conclusion about the impacts of land use and rainfall pattern.

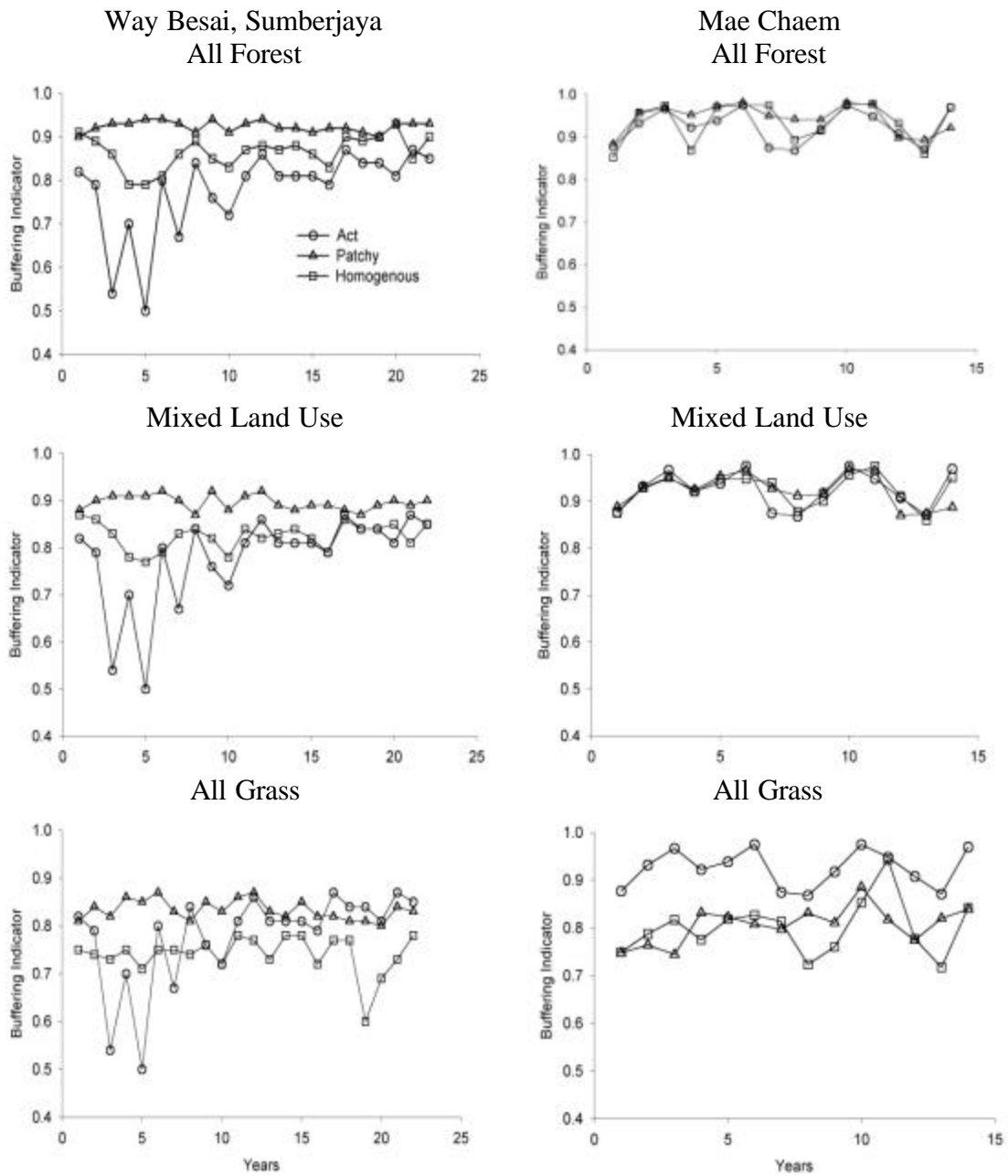


**Figure 3.41.** Buffer indicator over the year for different rainfall pattern and land use changes compare with actual data

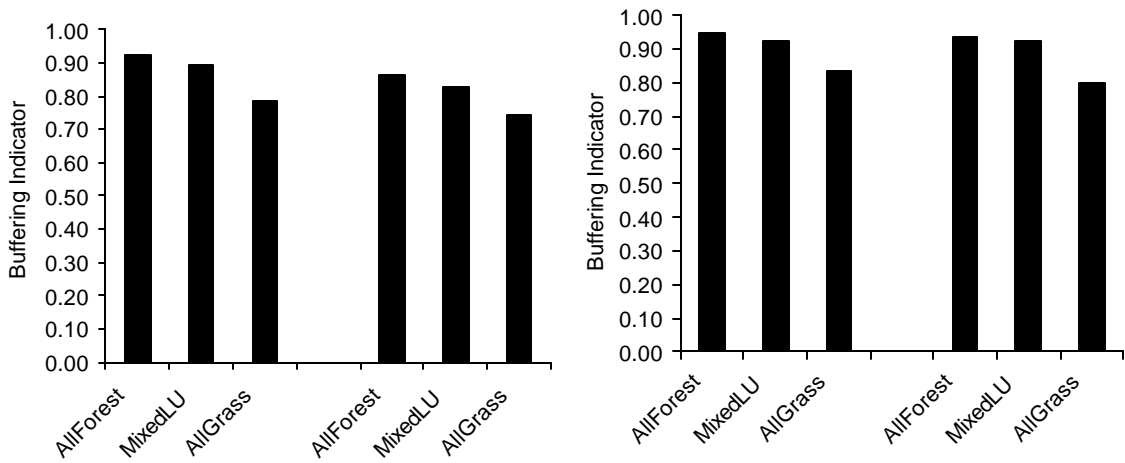


**Figure 3.42.** The mean annual buffering indicator of daily river flow as predicted from GenRiver model for Way Besai, Sumberjaya (left) and Mae Chaem (right)

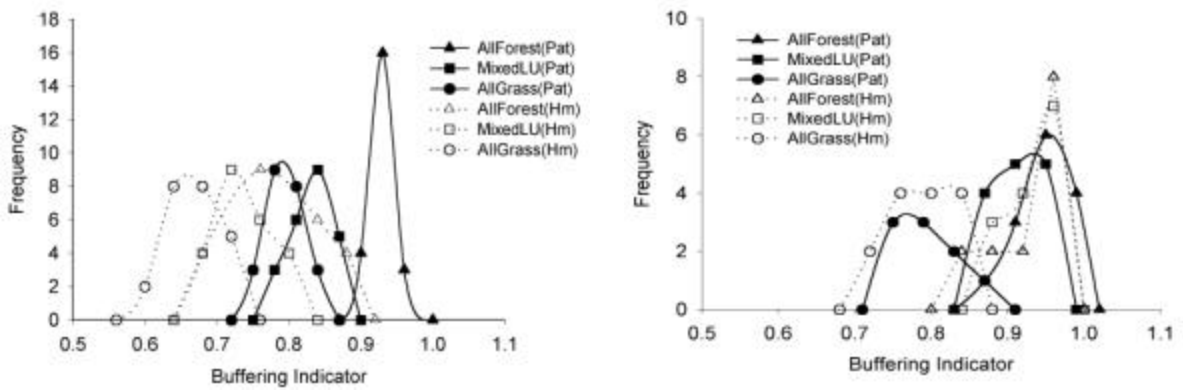


**Figure 3.43.** Frequency distribution of buffer indicator over 23 years period of the mean annual buffering indicator of daily river flow as predicted by GenRiver model for Way Besai (left; 20 years) and Mae Chaem (right; 14 years) under assumptions of patchy and homogenous rainfall pattern and all forest, mixed land use and grass land

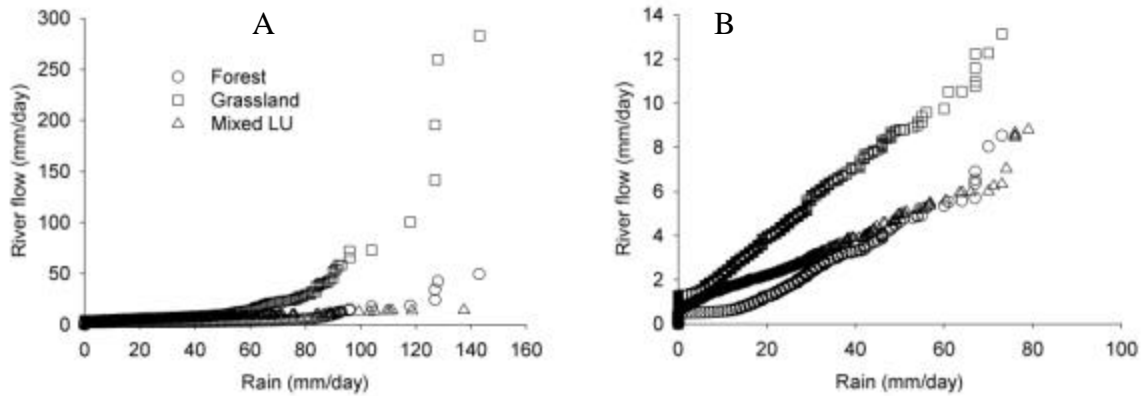


**Figure 3.44.** Rainfall and riverflow for Way Besai, Sumberjaya (A) and Mae Chaem (B) under assumption of forest, grassland and comparing with mixed land use (current land use)

### 3.5.3 Indicators of watershed functions

Overall, an acceptable agreement was obtained between measured and simulated values of the watershed function indicators for the current land use mosaic ('LU mix'), in the Way Besai (Table 3.7) and Mae Chaem (Table 3.8).

**Table 3.7** Indicators of watershed functions for Way Besai, comparing actual data (averaged over 20 years) with simulations for the current LU mix, an 'all forest' approximation of natural vegetation and an 'all grass' version of degraded lands, based on GenRiver simulations

Indicators	Actual Data	GenRiver		
	Current LU	Current LU	Natural Veg	Degraded land
Total Discharge Fraction	0.61	0.53	0.44	0.62
Buffering Indicator	0.79	0.82	0.80	0.68
Relative Buffering Indicator	0.66	0.66	0.55	0.49
Buffering peak events	0.86	0.81	0.76	0.78
Highest Monthly Discharge relative to mean rainfall	1.92	2.19	1.65	1.58
Lowest Monthly Discharge relative to mean rainfall	0.39	0.54	0.50	0.46
Overland Flow Fraction	*	0.11	0.00	0.36
Soil Quick Flow Fraction	*	0.10	0.02	0.00
Slow Flow Fraction	*	0.30	0.29	0.25

**Table 3.8.** Indicators of watershed functions for Mae Chaem, comparing actual data (averaged over 20 years) with simulations for the current LU mix, an ‘all forest’ approximation of natural vegetation and an ‘all grass’ version of degraded lands, based on GenRiver simulations

Indicators	Actual Data	GenRiver		
	Current LU	Current LU	Natural Veg	Degraded land
Total Discharge Fraction	0.21	0.19	0.13	0.32
Buffering Indicator	0.89	0.90	0.93	0.81
Relative Buffering Indicator	0.49	0.45	0.54	0.40
Buffering peak events	0.91	0.88	0.91	0.79
Highest Monthly Discharge relative to mean rainfall	3.16	3.67	3.01	3.37
Lowest Monthly Discharge relative to mean rainfall	0.20	0.22	0.27	0.24
Overland Flow Fraction	*	0.00	0.00	0.00
Soil Quick Flow Fraction	*	0.08	0.03	0.17
Slow Flow Fraction	*	0.14	0.08	0.12

### ***3.6 FALLOW predictions of impacts of forest positions within a landscape***

Forest protection in parts of watershed areas remains one of the main tools for ‘integrated watershed management’, but is often contested by farmers seeking livelihood options in these areas. According to Indonesia’s *Tata Guna Hutan Kesepakatan* (agreement on forests function allocation) around 30% of a catchment should be allocated as forest reserve (*hutan lindung*) in order to maintain hydrological functions. Existing criteria are criticized and the best spatial allocation of such ‘protection forest’ remains open to discussion, with options as riparian forest, steep slopes and the tops of ridges as candidates.

An analysis on the effectiveness of forest reserve allocation using the FALLOW Model was conducted for Sumberjaya area (see Suyamto et al, 2003 for more detail). This exercise is intended to explore the impacts of different rules for spatial allocation of forest reserve on watershed functions, expanding the analysis of Verbist et al. (2002) from hill slope and subcatchment scale to a landscape with interactive farmer decisions on land clearing. General attributes of the Sumber Jaya area used for the model parameterization were discussed by Verbist et al. (2002) and van Noordwijk et al. (2002). Five forested zones with the same allocation fraction of 0.25 were generated on the basis of a digital elevation model (DEM) of the area. The zones (Figure 2.35) are delineated according to distance to river with a threshold of 100 m nearby the river (riparian forests), steepness with threshold of 20% (sloping forests), elevation with threshold of 1000 m a.s.l. (ridge top forests), a uniformly random choice (random forests) and ‘remote forests’ at a distance to settlements of more than 1 km. Those zones are assigned as unchangeable zones over the whole simulation period, while the rest are dynamic.

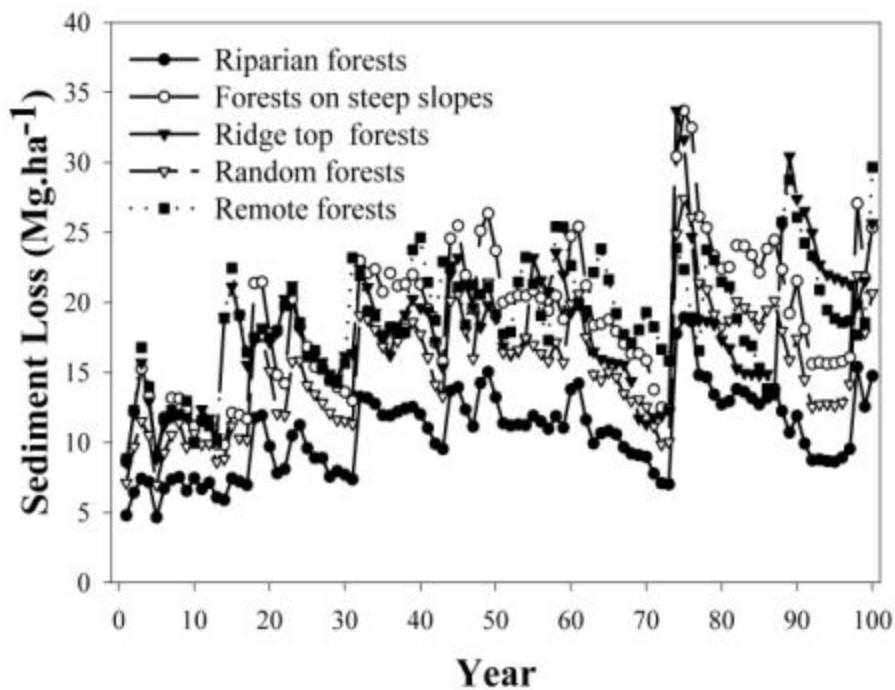


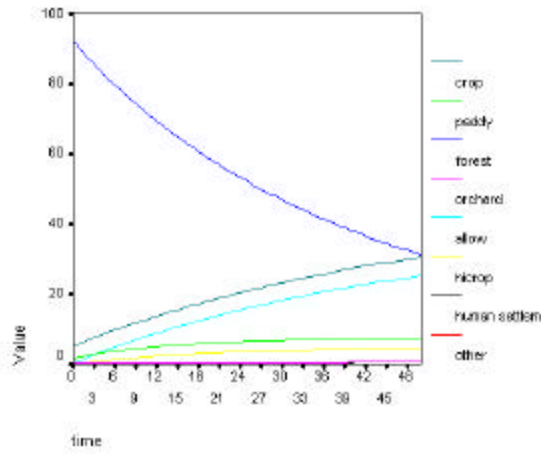
**Figure 3.45.** Simulated net sediment loss for a 100-year period (Mg.ha<sup>-1</sup>) resulted by five forest reserve allocation scenarios.

Based on simulation results over 100 years, riparian forests gave the lowest net sediment loss of the five patterns compared (Figure 3.45). The differences between the other forest locations tended to change with time. Variations with time in the simulation series depend on the stochastic nature of rainfall as well as dynamic decisions on land clearing depending on yields and the completion of production cycles.

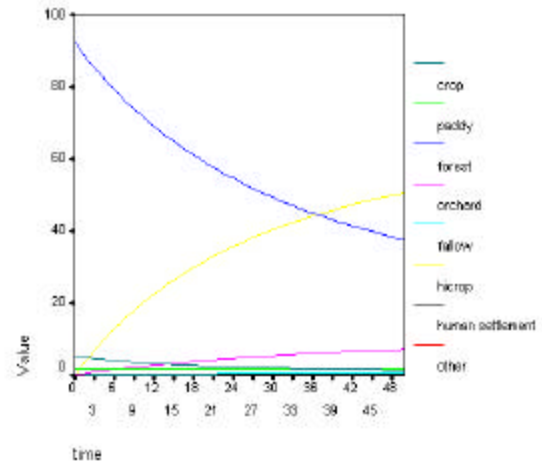
### ***3.7 Land use change scenarios for Mae Chaem***

#### ***3.7.1 Defining four scenarios for land use change***

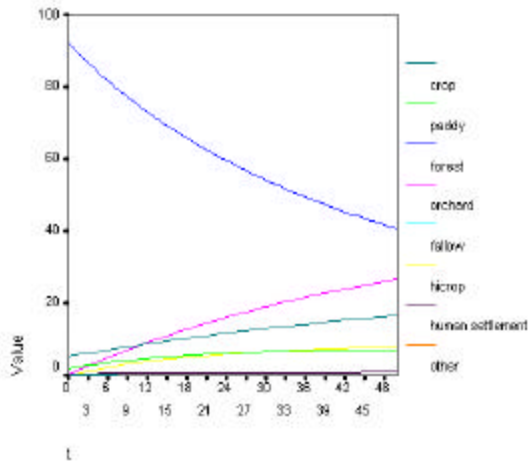
The simulation results with first version of the scenario-building model are summarized in a set of figures, describing land use change in response to a series of ‘drivers’ that modify the amount of tree & forest cover, as well as the degree of ‘segregation’ versus ‘integration’ of functions. As shown in Fig. 3.46 for almost all land cover types in all scenarios the changes were monotonic (either consistent increase or consistent decrease over the time period), so we can focus on the results after 50 years (Fig. 3.47) for a first indication of the consequences of these scenarios for the indicators of watershed functions.



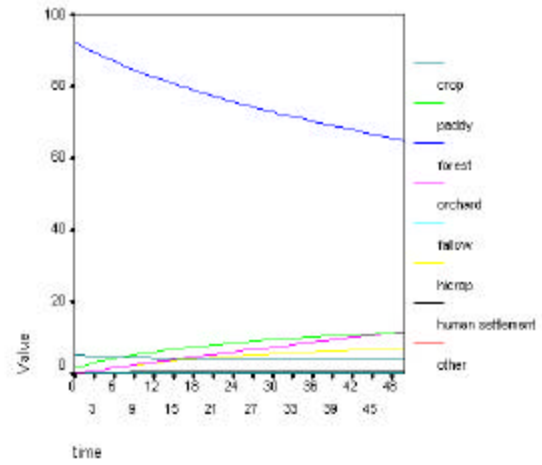
Fields & Fallows



Food Bowl



Agro - Forests



Parks

Figure 3.46. Aggregate land-cover changes in the five scenarios.

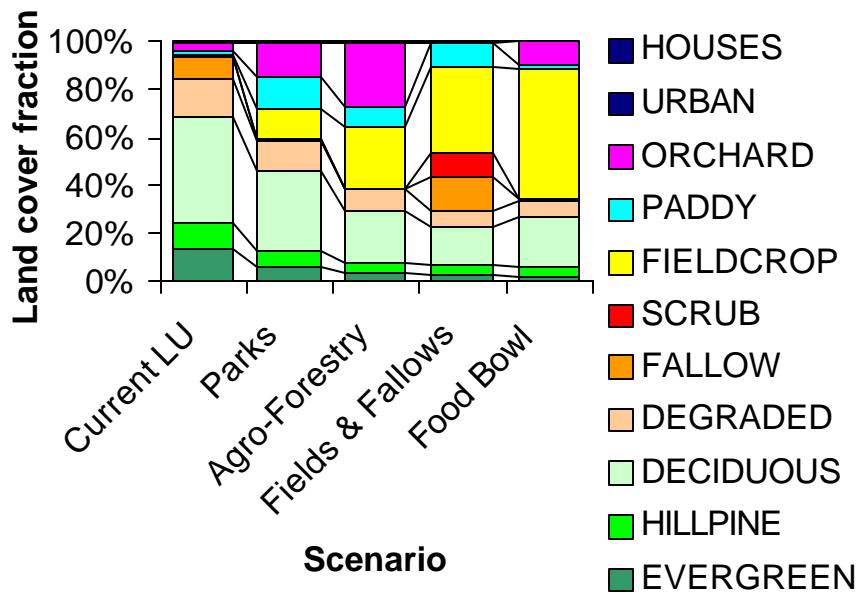
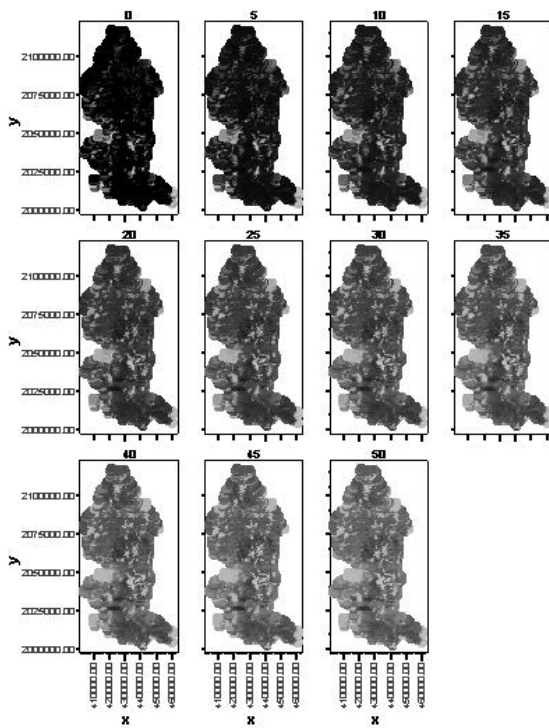


**Figure 3.47.** Predicted land cover fractions for Mae Chaem in year 50 for the four scenarios

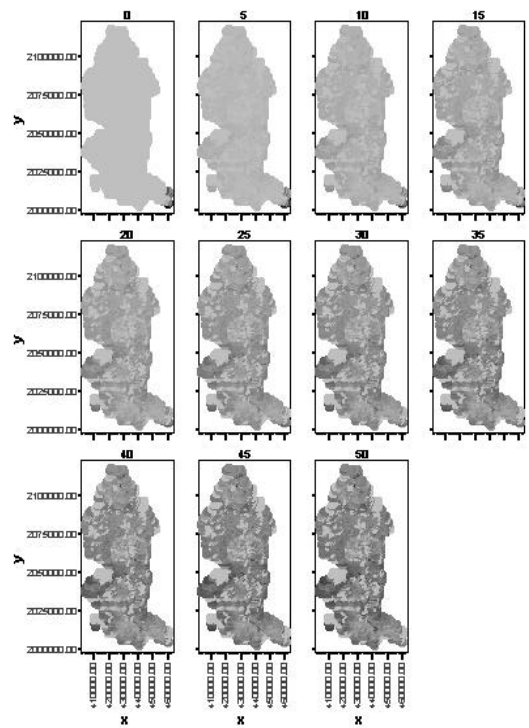
For all four scenarios the degree of forest cover is predicted to become less than the current one (Fig. 3.47), especially in the ‘evergreen’ forest type. The scenarios differ most clearly in the predicted fraction of land allocated to ‘field crops’ and ‘orchards’.

The simulation is explicit in the spatial configuration of these plausible land use change scenarios, with algorithms that reflect interactions between travel time, roads, elevation and competition between land covers (Figure 3.48, 3.49). The modeled landscape trajectories need to be interpreted within the qualitative context provided by the scenarios.

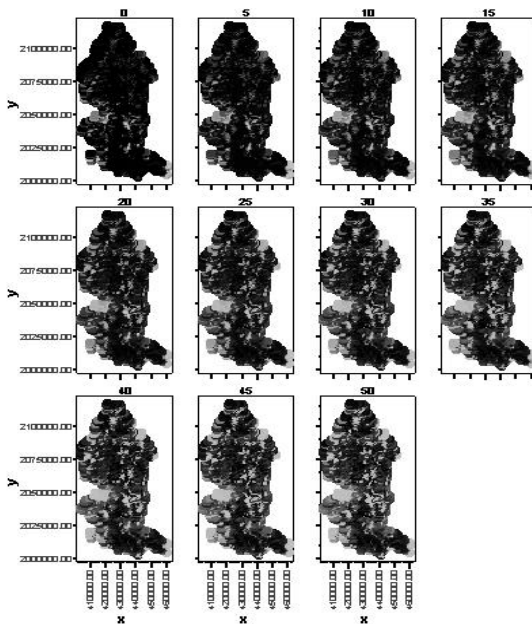
These simulations reflect ‘work in progress’. The next version of the model will refine the current results with four modeled processes: extension of the road network, extension and excisement of park area, the addition of new villages (above and beyond expansion of existing human settlements) and the expansion of irrigation. These additional processes are assumed to have very different characteristics in each of the scenarios. The next version of the model also includes spatial and temporal variability. Based on preliminary results with the road model these extensions create more complex temporal and spatial dynamics than the initial model.



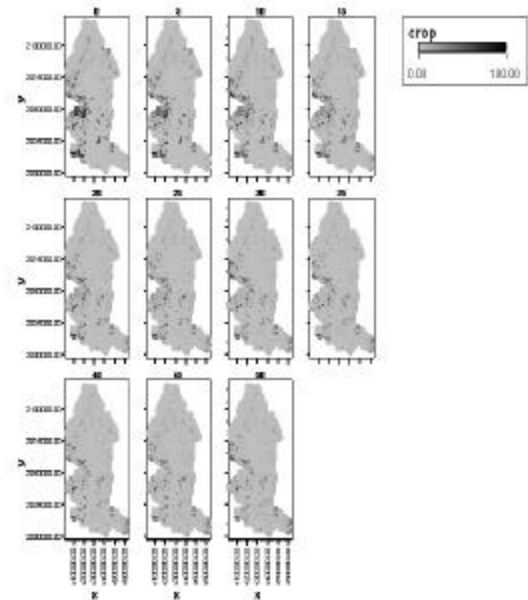
a. Forest Cover (Agro-forest Scenario)



b. Orchard Cover (Agro-forest Scenario)

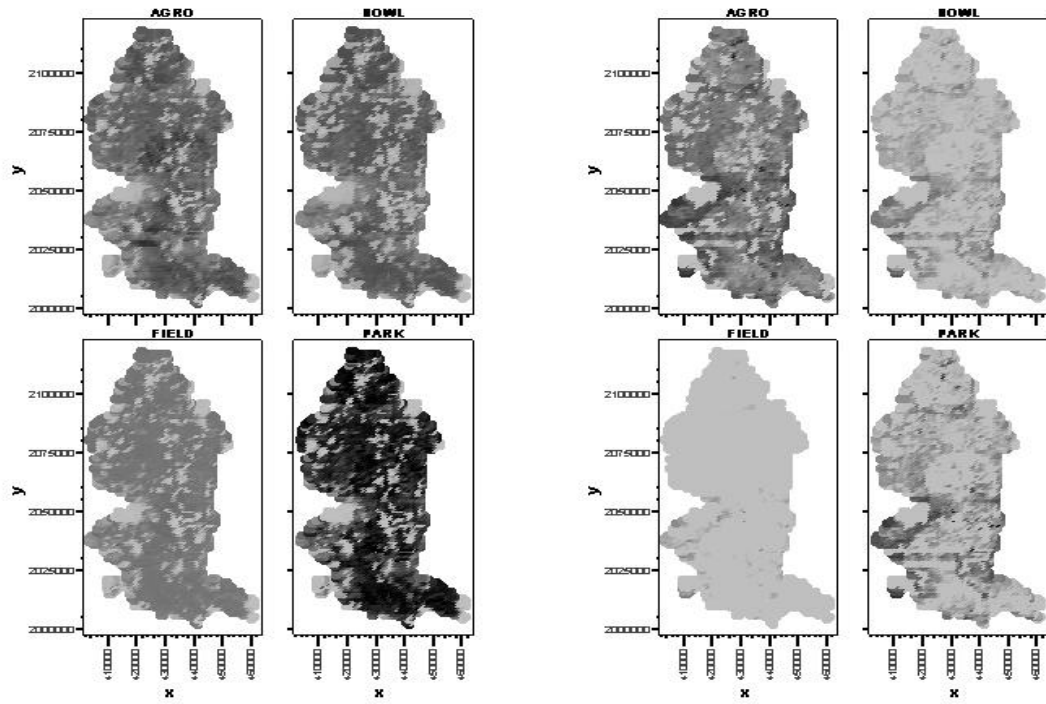


c. Forest Cover (Parks Scenario)



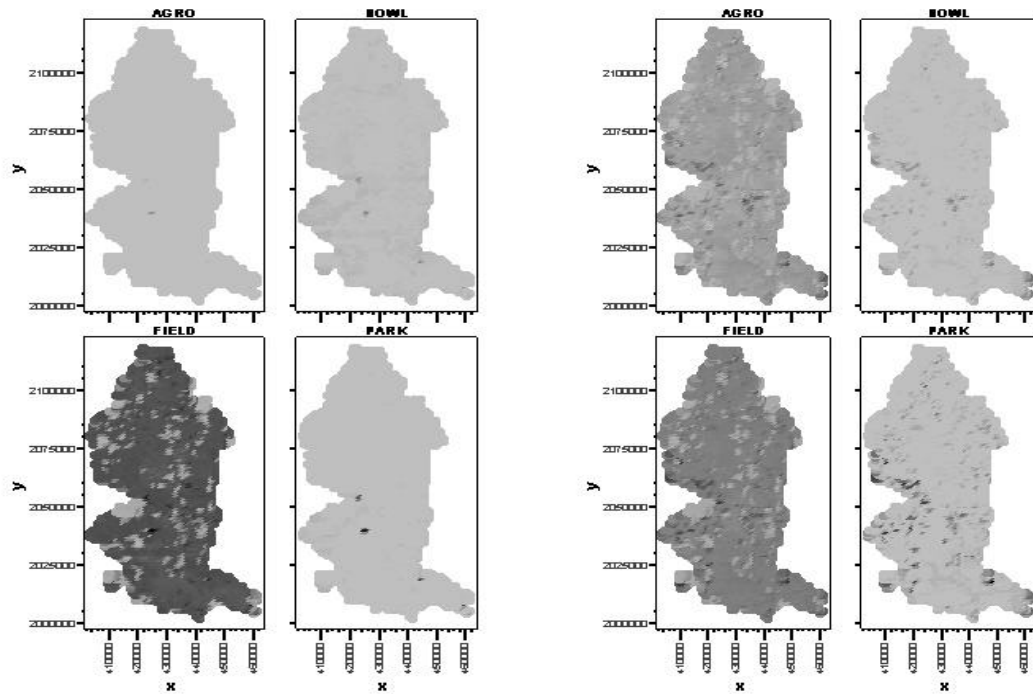
d. Field Crops (Parks Scenario)

**Figure 3.48.** Examples of changes in selected land covers in two of the scenarios



Forest

Orchard



Fallow

Crop

**Figure 3.49.** Comparison of final cover (at t = 50 years) in the four scenarios.

### 3.7.2 GenRiver simulations based on these four scenarios

**Table 3.9.** Indicators of Mae Chaem watershed functions under 4 plausible scenarios of land use change compared to the current land use mix, based on GenRiver simulations

Indicator	Current LU	Parks	Agro-Forest	Fields& Fallows	Food bowl
Total Discharge Fraction	0.19	0.25	0.28	0.33	0.38
Buffering Indicator	0.9	0.86	0.84	0.79	0.8
Relative Buffering Indicator	0.45	0.46	0.44	0.39	0.48
Buffering peak events	0.88	0.86	0.84	0.8	0.83
Highest Monthly Discharge relative to mean rainfall	3.67	3.06	3.12	3.24	2.77
Lowest Monthly Discharge relative to mean rainfall	0.22	0.24	0.24	0.21	0.25
Overland Flow Fraction	0	0	0	0	0.08
Soil Quick Flow Fraction	0.08	0.13	0.15	0.19	0.17
Slow Flow Fraction	0.14	0.10	0.11	0.12	0.11

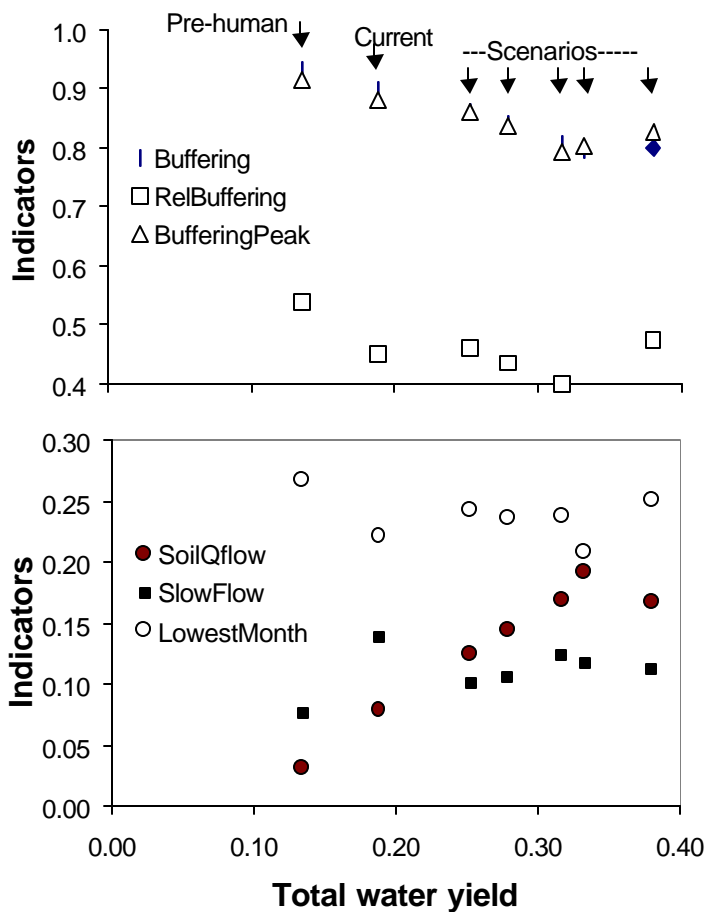


**Figure 3.50.** Quantitative indicators of watershed functions in Mae Chaem related to the total water yield indicator for the 'all forest', current LU mix' and plausible future scenarios